Abnormal Neural Differentiation in Response to Graphene Quantum Dots through Histone Modification Interference

Tingting Ku
Shanxi University
Zhihua Ren
Chinese Academy of Sciences
Renjun Yang
Chinese Academy of Sciences
Qian S. Liu
Chinese Academy of Sciences
Nan Sang
Shanxi University
Francesco Faiola
Chinese Academy of Sciences
Qunfang Zhou
zhouqf@rcees.ac.cn
Chinese Academy of Sciences
Guibin Jiang
Chinese Academy of Sciences

Research Article

Keywords: Graphene quantum dots, embryonic stem cells, neural differentiation, BMP signaling pathway, histone modification

Posted Date: July 5th, 2022

DOI: https://doi.org/10.21203/rs.3.rs-1767827/v1

Additional Declarations: No competing interests reported.

Version of Record: A version of this preprint was published at Environment International on December 1st, 2022. See the published version at https://doi.org/10.1016/j.envint.2022.107572.

Abstract

Background

Graphene quantum dots (GQDs) have been broadly applied in biomedicine in recent years, and their environmental exposure and toxicological impacts have raised increasing concerns. The nanosafety assessment on the nervous system is one of the most important aspects, and potential effects of GQDs on neurodevelopment and the underlying mechanism are still elusive. In this study, the neural developmental toxicities of hydroxylated GQDs (OH-GQDs) and amino functionalized GQDs (NH_2-GQDs) were investigated using the mouse embryonic stem cells (mESCs).

Results

The results revealed that OH-GQDs significantly inhibited the ectoderm development, and reduced the neural precursor formation and neurogenesis during the neural differentiation of the mESCs. The exploration on the mechanism uncovered that the increased enrichment of H3K27me3 at the promoter region of the *Smad6* gene was involved in histone modification-activated BMP signal pathway, which consequently influenced its regulatory effects on neural differentiation. Additionally, OH-GQDs elicited stronger effect on inducing the imbalance of histone modification, and resulted in higher latency of neural differentiation disturbance than did NH_2-GQDs, suggesting surface functionalization-specific effects of GQDs on neurodevelopmental toxicity.

Conclusion

This study would provide new insights in not only the adverse effects of GQDs on neurodevelopment, but also the influence from the chemical modification of GQDs on their bioactivities.

Background

With the rapid development and application of graphene quantum dots (GQDs), their exposure to the environment and human has been increasing in recent years [1]. Given the intentional or unintentional release of nanoparticles into the environment during their life cycle (e.g., during fabrication, use and disposal), the biological effects of these materials have attracted public attention [2, 3]. The currently-available studies have revealed the biosafety of GQDs, due to their low cytotoxicity in cell experiments [4, 5]. Moreover, to meet the needs of different applications, GQDs would be modified with abundant functional groups and used for supramolecular recognition [6]. For example, the amino groups can be covalently bonded to GQDs (NH_2-GQDs), facilitating the transformation from the ammonium moiety to the conjugated structure, making GQDs a more appropriate probe with superior sensitivity, selectivity, rapidity, and applicability [7]. Functionalizing GQDs with the hydroxyl group helps in the reverse of photoionization, improves surface stability, and increases the fluorescent yield-producing hydroxylated

GQDs (OH-GQDs) [8, 9]. However, the presence of functional groups might provide active sites for the subsequent occurrence of various biological reactions, and changes in the surface characteristics could enhance the risk uncertainty during the interaction of GQDs with organisms [10]. Therefore, it is urgent to study the biosafety of different chemically-modified GQDs.

The fetal origin of adult disease (FOAD) hypothesis proposes that an unfavorable environment during developmental stages can cause an increased risk of disease in adulthood [11]. Environmental irritants induce neurological damage and disease occurrence not only from direct exposure to adult proprioception, but may also be related to early neurodevelopmental changes. Nanoparticles have been reported even with the diameter of up to 240 nm were able to cross the blood-placenta barrier [12], including GQDs which can easily enter the target organs of the human body, affect germ cells [13] or affect embryonic development [14, 15, 16], and even cross the blood-brain barrier to reach and accumulate in the central nervous system (CNS) [17, 18], showing its potential reproductive and developmental toxicity. In addition, low-dose of N-GQD exposure could trigger microglial inflammation and induce mitochondrial iron death, while exposure to NH_2-GQD affected the olfactory transduction and GABAergic processes through several classic signaling pathways, including mTOR, ErbB and MAPK [19]. Meanwhile, some other artificial nanoparticles, such as titanium dioxide [20], silver [21], aluminum [22], and ultrafine particles [23] could also induce neurological developmental abnormalities, such as abnormal neurobehavior and axon growth in the offspring. These available data suggest that neurodevelopmental changes could be vulnerable to nanoparticle exposure, which offered an important aspect for studying the potential neurotoxicity of GQDs.

The development of the nervous system is a complex process, which is precisely regulated by a variety of factors, and its underlying mechanism study is challenging. To circumvent these obstacles, the technology of embryonic stem cells (ESCs) differentiation model provides powerful tools [24]. The ESCs can differentiate into various tissue cells under certain conditions, and the neural differentiation of the ESCs offer an important research window for exploring the mechanism for early development of nerves. In light of the importance of epigenetics in modulating ESC proliferation and differentiation fate, the entanglement of epigenetic mechanisms would be possible in GQD-induced biological effects on ESCs. Histone modifications closely relate to a mechanism of heritable changes in gene expression without changing DNA sequence, and is of proven importance in governing ESC pluripotency and differentiation [25]. Nevertheless, whether histone modifications are attributable to GQD-influenced neural differentiation of the ESCs remains to be determined.

Herein, based on the establishment of the neural differentiation model from the mouse ESCs (mESCs), the neurodevelopmental toxicities of two kinds of GQDs with the functional groups of hydroxyl and amino (i.e. OH-GQDs and NH_2-GQDs) were investigated, and the underlying histone modification-based mechanism was explored. The study attempted to provide new experimental evidences on the potential neurodevelopmental toxicities risk from the exposure to artificially-engineered GQDs.

Results And Discussion

Characterization of GQDs

The characterization for the physicochemical properties of GQDs showed that both OH-GQD and NH_2-GQD solutions emitted blue fluorescence under UV irradiation (Fig. 1A). The fluorescence spectrum scanning indicated that the maximum emission wavelength ($\lambda_{emission}$) was 425 nm for OH-GQD and NH_2-GQD, when the excitation wavelengths ($\lambda_{excitation}$) were controlled at 360 nm and 350 nm, respectively (Fig. 1B). NH_2-GQDs had relatively higher fluorescence efficiency than OH-GQDs. The morphological observation of both GQDs under the TEM displayed the similar spherical particles with well-resolved lattice fringes, and the average sizes were around 3 ~ 5 nm (Fig. 1C). The negatively-charged surfaces were found for these two test GQDs in cell culture medium, which could be attributed to the ionization of the oxygen-containing groups on GQD surfaces (Fig. 1D). The hydrodynamic diameter of OH-GQD and NH_2-GQDs were 237.50 nm and 167.93 nm, respectively (Fig. 1D), which were much larger than the particle sizes observed under the TEM (Fig. 1C), possibly due to the protein corona formation on the particles [26].

Cytotoxicologial effects of GQDs on the mESCs

To evaluate the cytological responses of the mESCs to two types of GQD exposure, the cytotoxicity was firstly measured, and the results showed that more than 80% of the cell viability remained under the test GQD concentrations (50 μg/mL or below) and exposure durations (24 h or 48 h) (Fig. 2A). The EdU incorporation assay showed that GQDs elicited little impact on the cell proliferation (Fig. 2B), which was consistent with the results from cell viability assay. The mESC colonies from different groups exhibited dark red after the AP staining (Fig. 2C), indicating neither OH-GQDs nor NH_2-GQDs affected the self-renewal property of the mESCs. These data were consistent with the previous finding [16], the surface functional groups of the test GQDs were different though.

Influences of GQDs on the tridermic development of the mESCs

A few studies based on germ cell and zebrafish models have reported GQDs might interfere with embryo development [14, 15], yet the consistent conclusions about the developmental toxicity of OH- or NH_2-GQDs have not been reached. To address that question, the *in vitro* differentiation of the mESCs was performed in the presence of OH-GQDs or NH_2-GQDs (0, 1, 10 μg/mL) for 4 or 9 days, and the analysis of the transcriptional expressions of the biomarkers for mesoderm (*Mesp1*, *Brachyury (T)*), endoderm (*Gata6*, *Sox17*), and ectoderm (*Fgf5*, *Krt14*) in the control groups showed that they were significantly increased along with the progress of the differentiation ($p < 0.05$, 0.01 or 0.001, Fig. 3), suggesting the successful embryoid body (EB) modeling. Nevertheless, the temporal variations were observed for some of the biomarkers like *T* and *Fgf5*, confirming the intricate regulation of the tridermic transcription network during the differentiation process.

In concern of GQD-induced effects, exposure to 10 μg/mL OH-GQD caused the significant induction in the mRNA levels of *Mesp1* and *Gata6* ($p < 0.05$ or 0.01, Fig. 3A, 3B), but decreased the transcriptional expression of *Fgf 5* (Fig. 3C). Of noteworthy, the inconsistent alterations were observed in the biomarkers for the three germ layers, as no significant changes were observed for *T*, *Sox17* or *Krt14* in any of OH-GQD exposure groups ($p > 0.05$, Fig. 3). The stimulation of the cells by 10 μg/mL NH_2-GQDs caused the significant increase in *Mesp1* on day 4, and decrease in *T* and *Krt14* on day 9 ($p < 0.05$ or 0.01, Fig. 3A, 3C). The disturbances in the tridermic development caused by these two GQDs showed their potential developmental toxicities, and the similar modulations on the ESC differentiation were also reported for some other environment pollutants, like arsenic trioxide [27], nicotine [28], etc. The consistent exposure concentration-dependent decreases in both *Fgf5* and *Krt14* induced by OH-GQDs at different time points (Fig. 3C) suggested the substantial interference in the ectodermal differentiation of the mESCs.

The inhibition of OH-GQDs on the neural differentiation of the mESCs

The ectoderm is the key initiating player in the embryogenesis of the CNS, which can be sub-specialized to form the neural ectoderm, and subsequently give rise to the brain, spinal cord, and peripheral nerves [29]. Previous studies have showed GQDs could reach and accumulate in the central nervous system (CNS) by passing through the blood-brain barrier, and result in severe neuronal disorders [17, 18]. The neurological injury might also be caused by the neurodevelopmental alterations induced by GQDs during the early stage of embryogenesis.

As evidenced by the disturbed ectoderm development due to OH-GQD exposure (Fig. 3C), the monolayer neural differentiation of the mESCs to the neural progenitor cell (NPCs) was further investigated for 12 days. The obvious morphological changes characterized by the neurofilament formation in Additional file 1: Figure **S1** confirmed the neural differentiation process was practically ongoing. The transcriptional analysis of the biomarkers for the neural precursor (*Sox1*, *Sox3*, *Pax6*) and neurogenesis (*Map2*, *NeuroD*, *Dcx*) in the control groups showed that they all gradually increased along with the neural differentiation of the mESCs, further demonstrating the substantial differentiation of the mESCs into the nerve cells (Fig. 4).

In the regard of GQD exposure, significant decreases were observed for *Sox1*, *Pax6*, *Map2* and *NeuroN* on differentiation day 12 in the cells with OH-GQD treatments ($p < 0.01$ or 0.001, Fig. 4), the slight stimulation was observed on differentiation day 6 though. Different from OH-GQDs, NH_2-GQDs showed no significant influence on the test biomarkers for the neural precursors or neurogenesis ($p > 0.05$, Fig. 4).

To further testify the consequence from GQD exposure on neural differentiation, the immunostaining of the neurofilament biomarkers, including Map2 and β-tubulin, was performed for the cells after 12-day differentiation, and the control group showed the extensive neurofilament connections probed by the green fluorescer (Fig. 5A), confirming the successful neural differentiation. In OH-GQD treatment, the reduced Map2 and β-tubulin expressions were indicated by relatively less numbers of green fluorescer-

probed synaptic contacts, in comparison with those in the control group (Fig. 5A). The western blotting analysis of Map2 also showed the significant reduction of this protein level in the differentiated cells following 12-day OH-GQD exposure at the concentration of 10 μg/mL ($p < 0.05$, Fig. 5B). Distinct from OH-GQDs, the exposure to NH_2-GQDs did not compromise the neural differentiation of the mESCs, as evidenced by the unchanged expressions of Map2 and β-tubulin from both the immunostaining assay and western blotting analysis (Fig. 5). The above results for the protein biomarker analysis were well consistent with the transcriptional data in Fig. 4.

It is known that Map2 plays a critical role in regulating cytoskeleton dynamics [30], and the inhibition of Map2 expression induced by OH-GQDs suggested that this kind of nanoparticle could influence the neurite outgrowth and synaptic plasticity. Likely, silver nanoparticles were also reported to induce toxicities to the neuron and astrocyte network though disrupting Map2 expression [31], suggesting the dysregulation of Map2 could be involved in some nanoparticles-induced neurotoxicities.

The Effect of OH-GQDs on the Histone Modification-Activated BMP Signaling

It is well known that the bone morphogenetic protein (BMP) belongs to the transforming growth factor (TGF-β) superfamily, which is not only directly related to early neural fate determination, but also plays a very important role in the proliferation and differentiation of the neural stem cells and the formation of various subtypes of cells in the nervous system [32]. The BMP signaling pathway was thus further interrogated to reveal the mechanism underlying OH-GQD-compromised neural differentiation. The transcriptional analysis of the major intracellular components in BMP signaling (i.e. *Smad6*, *Smad9* and *Id3*) in the control groups showed that they were increasingly expressed along with the differentiation duration (Fig. 6A). The evaluation for the phosphorylation of Smads revealed that the cellular level of p-Smad1/5/9 was significantly increased on differentiation day 12 ($p < 0.001$, Fig. 6B). These results suggested the regulatory role of BMP signaling in different stages of neurodevelopmental process.

In terms of GQD exposure, OH-GQDs significantly reduced *Smad 6* expression on differentiation day 12 ($p < 0.01$), while they exhibited induction effects on the test biomarkers on differentiation day 6 (Fig. 6A). However, no influence was observed following NH_2-GQDs exposure (Fig. 6A). Similarly, the exposure to 10 μg/mL OH-GQDs caused the significant decrease in the phosphorylation of Smads ($p < 0.05$), while NH_2-GQDs showed no effects (Fig. 6B).

Studies have shown that the BMP signaling pathway plays different, sometimes even opposite, roles in different periods of neural differentiation [33]. The inhibition of BMP signaling is required during neural induction [34], while it plays a positive regulatory role in the formation of neural precursor cells [35]. As shown in Fig. 6A and 6B, OH-GQDs interfered with BMP signaling at different stages of neural differentiation. Smad6, as a negative regulator of BMP signaling, is required for promoting NPCs to exit the cell cycle and differentiate into neurons [36], and it also promotes the formation of Map2-expressed cells [37]. The findings herein showed that the expressions of both Map2 and Smad6, together with the

phosphorylation of Smads, were dramatically induced along with the neural differentiation process. Nevertheless, OH-GQD exposure reduced the expressions of Map2, Smad6 and p-Smad1/5/9, causing the consequent inhibition of the neural differentiation.

The histone apparent modification has been found to regulate the BMP signaling pathway, and influence the process of neurodevelopment [38]. The plausible molecular basis for OH-GQD-induced inhibition in neural differentiation was thus explored by testing the histone modification of Smad6. According to the result from the ChIP-*q*PCR assay, the global H3K27me3 level within the promoter regions of Smad6 was significantly increased after the neural differentiation of the mESCs ($p < 0.05$, Additional file 1: Figure **S2**), accompanying with the increase in Smad6 expression during this process (Fig. 6A). As for GQD treatments, neither OH-GQDs nor NH_2-GQDs showed any influences on the global level of H3K27me3 (Additional file 1: Figure **S2**). However, the enrichment of H3K27me3 at the promoter region of the Smad6 gene was significantly increased following OH-GQD exposure ($p < 0.05$, Fig. 6C), which could explain the consequent repression in Smad6 expression (Fig. 6A**)** due to the condensed enrichment of H3K27me3.

In the regard of surface functional modification-related effect, OH-GQDs showed stronger effect on inducing the imbalance of histone modification and neural differentiation disturbance than did NH_2-GQDs, showing the potential role of the surface hydroxyl group on GQDs in delaying the neural precursor formation. Previous studies also indicated that neurotoxic potential of the graphene family nanomaterials followed the order: G-OH > G-NH_2 [39]. The lower toxicity observed for NH_2-GQDs herein was consistent with the previous study that aminated graphene was more favorable for neurite outgrowth and branching [40]. The amino group functionalization was capable of promoting the linkage between graphene materials and organic molecules, and reducing the charge transfer to cells [41, 42], suggesting the relatively high biological compatibility.

Conclusion

Altogether, OH-GQD and NH_2-GQDs could affect the global differentiation of the mESCs, especially for inhibiting the ectoderm development. Moreover, OH-GQD could selectively suppress Map2 expression through histone modification-regulated BMP signaling pathway by increasing the enrichment of H3K27me3 at the promoter region of the *Smad6* gene, resulting in the delayed neural precursor formation and neurogenesis (Fig. 7). This study highlighted the importance in the biosafety evaluation of so called low-toxic QDs to ensure an unbiased and mechanism-based risk assessment of nanoimpact.

Material And Methods

Materials

Two kinds of GQDs (i.e. OH-GQDs and NH_2-GQDs) were purchased from Xianfeng Nanotechnology Co., Ltd. (Nanjing, China), and their suspensions in water (1 mg/mL and 20 mg/mL, respectively) were used

as the stock solutions, and stored in the dark at 4 °C. The working solution was freshly prepared under the sterile condition by diluting with the cell culture medium.

Characterization of GQDs

The morphology of the test GQDs was visualized, using a high-resolution transmission electron microscopy (TEM, JEM-F20, Japan) at the acceleration voltage of 200 kV. Their zeta potentials and hydrodynamic sizes in N2B27 medium at the concentration of 50 μg/mL were analyzed by a Malvern Zetasizer Nano ZS (Malvern, UK) to accord with the cell experiments in the following studies. The fluorescence spectrum of these two GQDs were scanned using a fluorescence spectrophotometer (F-7000, Hitachi, Japan) at the excitation wavelength in the range of 340–410 nm.

Cell culture

The J1 mESCs (Shanghai Institute of Biochemistry and Cell Biology, Chinese Academy of Sciences) were seeded on 0.1% gelatin (Millipore, USA) pre-coated 96-well, 12-well or 6-well plates at the densities of 1×10^4, 1×10^5, and 2×10^5 cells per well, respectively, and cultured in KSR medium at 37 ℃ under 5% CO_2 for 12 h to obtain cell attachment on the plates. Then, the KSR medium was replaced with N2B27 medium for the proliferation and colony formation of the mESCs [43]. The experiments based on the mESCs were performed by adding different concentrations of GQDs in N2B27 medium, and the duration lasted for 24 h or 48 h. The naïve ESCs were also tested throughout the study as the undifferentiated control for evaluating the neural committed differentiation process.

Cell viability

The mESCs cultured in 96-well plates were exposed to a series of concentrations of OH-GQDs or NH_2-GQDs (0, 1, 10, 50 μg/mL) for 24 h and 48 h, respectively. When the exposure was terminated, the cells were incubated with the fresh N2B27 medium containing 10 μM alamarBlue (Thermo Fisher Scientific, USA) for 2 h at 37°C in the dark, and the absorbance at the wavelength of 490 nm was recorded using a microplate reader (VARIOSKAN FLASH, Thermo Fisher Scientific, USA). The non-cytotoxic levels of GQDs based on the results of this assay were selected for the following mESC experiments.

EdU incorporation assay

The cellular proliferation of the mESCs was evaluated by EdU incorporation method. Briefly, the mESCs were exposed to different concentrations of GQDs (0, 1, 10 and 50 μg/mL) for 48 h, and the probe of EdU (2.5 μM) was added to the exposure systems and incubated for 2 h to label the S-phase cells with DNA replication. Then, the cells were harvested, fixed, permeabilized, and stained in accordance with the manufacturer's instructions (RiboBio, China). The quantitative analysis of apollo 567-labeled EdU-positive cells in different exposure groups were examined using a flow cytometry (NovoCyte, Agilent Technologies, USA).

Alkaline phosphatase (AP) activity

According to the previously-reported protocol [43], the mESCs were submitted to 48-h GQD exposure (0, 1, 10 and 50 μg/mL) in 12-well plates, and then fixed with citrate-acetone-formaldehyde buffer, incubated with alkaline-dye mixture and finally counterstained with hematoxylin solution using the AP kit (Sigma, USA). The morphology of the cell colonies from different exposure groups was observed under the inverted microscope (Olympus IX73, Japan), and the representative images were taken from different visual fields.

EB formation assay

In vitro differentiation of the mESCs into EBs was performed according to the protocol reported previously [44]. Briefly, the mESCs were passaged using 0.05% TrypLE express enzyme, seeded onto ultra-low attachment 6-well plates (Corning, USA) at the density of $4{\cdot}10^5$ cells per well, and cultured in 2 mL of differentiation medium containing 1 and 10 μg/mL OH-GQDs or NH_2-GQDs. The controls without GQD treatment were also designed, and the differentiation medium was replaced every other day during EB formation. The EB samples were collected on differentiation day 4 and 9 for the subsequent characterization of three germ layers using the quantitively polymerase chain reaction (*q*PCR) assay. The mESCs were also tested as the undifferentiated control.

Neural differentiation of the mESCs

Briefly, the mESCs ($8{\times}10^4$ cells per well) were seeded onto 0.1% gelatin-coated 6-well plates, and cultured in N2B27 medium consisted of 50% DMEM/F12 and 50% Neurobasal™ medium (Gibco, USA), supplemented with 0.1% bovine serum albumin fraction V (Beyotime, China), 1× N2 supplement, 1× B27 supplement (Gibco, USA), 0.1 mM β-mercaptoethanol and 1% GlutaMax). The neural differentiation media was changed every other day, and the exposure experiments were performed by culturing the mESCs in the neural differentiation media, containing different levels of OH-GQDs or NH_2-GQDs. The cell samples exposed to 10 μg/mL GQDs were collected on differentiation day 2, 6 or 12 for nerve formation and BMP signaling evaluation, using *q*PCR. The cells harvested from GQD treatments at different exposure levels (0, 1, 10 μg/mL) on neural differentiation day 12 were submitted to immunofluorescence staining, chromatin immunoprecipitation (ChIP) analysis or western blotting. The mESCs were concomitantly tested for the comparison with the neural differentiated cells.

Immunofluorescence staining

The neural cells from the committed differentiation of the mESCs on day 12 were fixed, and incubated overnight with MAP2 (1:50, Cell Signaling Technology, USA) or β3 Tubulin antibodies (1:50, Santa Cruz Biotechnology, USA). Then the cells were immunoblotted with Alexa fluorescently-labeled IgG antibody (1:1000, Proteintech, China) for 1 h, and finally stained with DAPI. The representative images were captured under different visual fields using a fluorescence microscope (Olympus IX83, Japan).

The qPCR analysis

Total RNA samples were extracted from different treatments described above using the TRIzol Reagent (Gibco, USA), and submitted to the synthesis of first-strand complementary DNA (cDNA) with a reverse

transcription kit (BioRad, USA). The quantification of the target gene expressions was carried out using SYBR Green *q*PCR Master Mix (BioRad, USA) on Roche 480 Real-Time PCR system (Roche, USA). The relative transcriptional levels of the biomarkers for EB formation (*Mesp1*, *Brachyury T*, *Gata6*, *Sox17*, *Fgf5* and *Krt14*), neural differentiation (*Sox1*, *Sox3*, *Pax6*, *Map2*, *NeuroN* and *Dcx)* and BMP signaling (*Smad6*, *Smad9* and *Id3*) were normalized to that of *GAPDH*, using the method of $2^{-\triangle\triangle CT}$, and the primer sequences for these test genes were listed in Additional file 1: Table **S1**.

Western blotting assay

The cell samples after 12-day neural differentiation, together with the undifferentiated mESCs, were lysed with RIPA solution (Solarbio, China). The extracted proteins were subsequently separated by the sodium dodecyl sulfate (SDS)-polyacrylamide gel electrophoresis (PAGE), and transferred to a PVDF membrane. The target proteins were investigated by the overnight incubation of the membrane with the corresponding primary antibodies, including anti-Map2, anti-Smad1, anti-p-Smad1/5/9, anti-H3K27me3 (1:1000, Cell Signaling Technology, USA) or anti-GAPDH (1:2500, Abcam, USA). The horseradish peroxidases (HRP)-labeled secondary antibody (1:2500, ZSGB-BIO, China) were subsequently used. The quantitative analysis of the target protein expressions was performed by adjusting with the corresponding GAPDH levels.

Chromatin immunoprecipitation (ChIP) analysis

The ChIP analysis was performed to investigate the enrichment of H3K27me3 at the Smad6 promoter, according to the manufacturer's instructions (Cell Signal Technology, USA). The pair primer sequences for the ChIP were listed in Additional file 1: Table **S1** for the binding site. Briefly, the cells from different treatments were fixed with formaldehyde to cross-link DNA and proteins. After the wash with cold PBS twice, the cells were lysed with SDS buffer, and the genomic DNA was sonicated into fragments. After the incubation with the antibodies against IgG or H3K27me3, DNA was purified and amplified by the specific primers (Additional file 1: Table **S1**) using *q*PCR assay.

Statistical analysis

All the experiments were independently performed for 3 times or more. The data from different treatments were presented as the mean ± SE, and analyzed with one-way ANOVA followed by LSD's post hoc analysis. The significant differences were considered in all tests, when p value was less than 0.05, 0.01, or 0.001.

Abbreviations

GQDs: Graphene quantum dots; mESCs: mouse embryonic stem cells; NH_2-GQDs: amino functionalized GQDs; OH-GQDs: hydroxylated GQDs; FOAD: The fetal origin of adult disease; CNS: central nervous system; ESCs: embryonic stem cells; $\lambda_{emission}$: the emission wavelengths; $\lambda_{excitation}$: excitation wavelengths; EB: embryoid body; NPCs: neural progenitor cell; BMP: bone morphogenetic protein; TGF-β: the transforming growth factor; TEM: transmission electron microscopy; AP: Alkaline phosphatase; *q*PCR:

quantitively polymerase chain reaction; ChIP: chromatin immunoprecipitation; cDNA: complementary DNA; SDS: sodium dodecyl sulfate; PAGE: polyacrylamide gel electrophoresis; HRP: horseradish peroxidases.

Declarations

Ethics approval and consent to participate

Not applicable.

Consent for publication

Not applicable.

Availability of data and materials

All data analyzed within this study are included either in the manuscript or in the Additional File.

Competing interests

The authors declare no competing financial interests.

Funding

This research was supported by National Key R&D Program of China (2018YFA0901101), National Natural Science Foundation of China (22193050, 91943301, 22176203, 22176119, 21806094) and the China Postdoctoral Science Foundation (2018M641493).

Authors' contributions

TTK was responsible for the study design and the manuscript writing. ZHR and RJY contributed to cell model building. QSL helped with data analysis. NS and FF reviewed and edited the manuscript. QFZ and GBJ supervised this research project. All authors read and approved the final manuscript.

Acknowledgements

Not applicable.

Author details

[1]State Key Laboratory of Environmental Chemistry and Ecotoxicology, Research Center for Eco-Environmental Sciences, Chinese Academy of Sciences, Beijing 100085, China. [2]College of Environment and Resource, Research Center of Environment and Health, Shanxi University, Taiyuan, 030006, China. [3]College of Resources and Environment, University of Chinese Academy of Sciences, Beijing 100049, China. [4]Institute of Environment and Health, Jianghan University, Wuhan 430056, China

References

1. Cy A, Xuan GA, B X, Zy A, Jj C. Transport of graphene quantum dots (GQDs) in saturated porous media. Colloids Surf A. 2020;589:124418.
2. Hicks AL, Dysart AD, Pol VG. Environmental impact, life cycle analysis and battery performance of upcycled carbon anodes. Environ Sci: Nano. 2018;5:1237-1250.
3. Kang W, Li X, Sun A, Yu F, Hu X. Study of the persistence of the phytotoxicity induced by graphene oxide quantum dots and of the specific molecular mechanisms by integrating omics and regular analyses. Environ Sci Technol. 2019;53(7):3791-801;
4. Fasbender S, Zimmermann L, Cadeddu RP, Luysberg M, Moll B, Janiak C, et al. The low toxicity of graphene quantum dots is reflected by marginal gene expression changes of primary human hematopoietic stem cells. Sci Rep. 2019;9(1):12028.
5. Zhang D, Wen L, Huang R, Wang H, Hu X, Xing D. Mitochondrial specific photodynamic therapy by rare-earth nanoparticles mediated near-infrared graphene quantum dots. Biomaterials. 2018;153:14-26.
6. Mansuriya BD, Altintas Z. Applications of Graphene Quantum Dots in Biomedical Sensors. Sensors (Basel, Switzerland). 2020;20 (4): 1072-1142.
7. Zhu X, Yu J, Yan Y, Song W, Hai X. One-pot alkali cutting-assisted synthesis of fluorescence tunable amino-functionalized graphene quantum dots as a multifunctional nanosensor for sensing of pH and tannic acid. Talanta. 2022;236:122874.
8. Geethalakshmi KR, Teng YN, Crespo-Otero RJJoMCC. Tunable optical properties of OH-functionalised graphene quantum dots. J Mater Chem C. 2016;4(36): 8429.
9. Anas NAA, Fen YW, Yusof NA, Omar NAS, Ramdzan NSM, Daniyal W. Investigating the properties of cetyltrimethylammonium bromide/hydroxylated graphene quantum dots thin film for potential optical detection of heavy metal ions. Materials. 2020;13(11):2591.
10. Deng S, Fu A, Junaid M, Wang Y, Yin Q, Fu C, et al. Nitrogen-doped graphene quantum dots (N-GQDs) perturb redox-sensitive system via the selective inhibition of antioxidant enzyme activities in zebrafish. Biomaterials. 2019;206:61-72.
11. Barker DJ. The fetal and infant origins of adult disease. BMJ. 1990;301(6761):1111.
12. Lan Z, Yang WX. Nanoparticles and spermatogenesis: how do nanoparticles affect spermatogenesis and penetrate the blood-testis barrier. Nanomedicine. 2012;7(4):579-96.
13. Li P, Xu T, Wu S, Lei L, He D. Chronic exposure to graphene-based nanomaterials induces behavioral deficits and neural damage in Caenorhabditis elegans. J Appl Toxicol. 2017;37(10):1140-50.
14. Ji X, Xu B, Yao M, Mao Z, Zhang Y, Xu G, et al. Graphene oxide quantum dots disrupt autophagic flux by inhibiting lysosome activity in GC-2 and TM4 cell lines. Toxicology. 2016;374:10-7.
15. Zhang JH, Sun T, Niu A, Tang YM, Deng S, Luo W, et al. Perturbation effect of reduced graphene oxide quantum dots (rGOQDs) on aryl hydrocarbon receptor (AhR) pathway in zebrafish. Biomaterials. 2017;133:49-59.

16. Ku T, Hao F, Yang X, Rao Z, Liu QS, Sang N, et al. Graphene quantum dots disrupt embryonic stem cell differentiation by interfering with the methylation level of sox2. Environ Sci Technol. 2021;55(5):3144-55.
17. Wang H, Revia R, Mu Q, Lin G, Yen C, Zhang M. Single-layer boron-doped graphene quantum dots for contrast-enhanced in vivo T(1)-weighted MRI. Nanoscale horiz. 2020;5(3):573-9
18. Kim D, Yoo JM, Hwang H, Lee J, Lee SH, Yun SP, et al. Graphene quantum dots prevent α-synucleinopathy in Parkinson's disease. Nat Nanotechnol. 2018;13(9):812-8.
19. Wu T, Li Y, Liang X, Liu X, Tang M. Identification of potential circRNA-miRNA-mRNA regulatory networks in response to graphene quantum dots in microglia by microarray analysis. Ecotoxicol Environ Saf. 2021;208:111672.
20. Gu J, Guo M, Huang C, Wang X, Zhu Y, Wang L, et al. Titanium dioxide nanoparticle affects motor behavior, neurodevelopment and axonal growth in zebrafish (Danio rerio) larvae. Sci Total Environ. 2021;754:142315.
21. Abdelkhaliq A, van der Zande M, Peters RJB, Bouwmeester H. Combination of the BeWo b30 placental transport model and the embryonic stem cell test to assess the potential developmental toxicity of silver nanoparticles. Part Fibre Toxicol. 2020;17(1):11.
22. Ding Y, Jia LN, Yang B, Zhang G, Wang HY, Guo WW, et al. Effects of maternal exposure to nano-alumina during pregnancy on neurodevelopment in offspring mice. Chin J Ind Hyg Occup Dis. 2013;31(10):744-8.
23. Haghani A, Johnson R, Safi N, Zhang H, Thorwald M, Mousavi A, et al. Toxicity of urban air pollution particulate matter in developing and adult mouse brain: Comparison of total and filter-eluted nanoparticles. Environ Int. 2020;136:105510.
24. Haremaki T, Metzger JJ, Rito T, Ozair MZ, Etoc F, Brivanlou AH. Self-organizing neuruloids model developmental aspects of Huntington's disease in the ectodermal compartment. Nat Biotechnol. 2019;37(10):1198-208.
25. Liu P, Dou X, Liu C, Wang L, Xing C, Peng G, et al. Histone deacetylation promotes mouse neural induction by restricting Nodal-dependent mesendoderm fate. Nat Commun. 2015;6:6830.
26. Xu M, Yang Q, Xu L, Rao Z, Cao D, Gao M, et al. Protein target identification and toxicological mechanism investigation of silver nanoparticles-induced hepatotoxicity by integrating proteomic and metallomic strategies. . Part Fibre Toxicol. 2019;16(1):46.
27. Yuan W, Chen J, Huang H, Cai Z, Ling Q, Huang F, et al. Low-dose arsenic trioxide modulates the differentiation of mouse embryonic stem cells. Chem Res Toxicol. 2018;31(6):472-81.
28. Guo H, Tian L, Zhang JZ, Kitani T, Paik DT, Lee WH, et al. Single-cell rna sequencing of human embryonic stem cell differentiation delineates adverse effects of nicotine on embryonic development. Stem cell reports. 2019;12 4:772-86.
29. Dash S, Bhatt S, Sandell LL, Seidel CW, Ahn Y, Krumlauf RE, et al. The mediator subunit, med23 is required for embryonic survival and regulation of canonical wnt signaling during cranial ganglia development. Front Physiol. 2020;11:531933.

30. Hrstka SCL, Ankam S, Agac B, Klein JP, Moore RA, Narapureddy B, et al. Proteomic analysis of human iPSC-derived sensory neurons implicates cell stress and microtubule dynamics dysfunction in bortezomib-induced peripheral neurotoxicity. Exp Neurol. 2021;335:113520.
31. Repar N, Li H, Aguilar JS, Li QQ, Drobne D, Hong Y. Silver nanoparticles induce neurotoxicity in a human embryonic stem cell-derived neuron and astrocyte network. Nanotoxicology. 2018;12(2):104-16.
32. Jovanovic VM, Salti A, Tilleman H, Zega K, Jukic MM, Zou H, et al. BMP/SMAD pathway promotes neurogenesis of midbrain dopaminergic neurons in vivo and in human induced pluripotent and neural stem cells. J Neurosci. 2018;38 7:1662-76.
33. Niwa H. How is pluripotency determined and maintained? Development. 2007;134(4):635-46.
34. Piacentino ML, Hutchins EJ, Bronner ME. Essential function and targets of BMP signaling during midbrain neural crest delamination. Dev Biol. 2021;477:251-61.
35. Katada S, Takouda J, Nakagawa T, Honda M, Igarashi K, Imamura T, et al. Neural stem/precursor cells dynamically change their epigenetic landscape to differentially respond to BMP signaling for fate switching during brain development. Genes Dev. 2021;35 21-22:1431-44.
36. Xie Z, Chen Y, Li Z, Bai G, Zhu Y, Yan R, et al. Smad6 promotes neuronal differentiation in the intermediate zone of the dorsal neural tube by inhibition of the Wnt/beta-catenin pathway. Proc Natl Acad Sci U S A. 2011;108(29):12119-24.
37. Fang H, Song P, Shen C, Liu X, Li H. Bone mesenchymal stem cell-conditioned medium induces the upregulation of Smad6, which inhibits the BMP-4/Smad1/5/8 signaling pathway. Neurol Res. 2016;38(11):965-72.
38. Wang J, Yang L, Dong C, Wang J, Xu L, Qiu Y, et al. EED-mediated histone methylation is critical for CNS myelination and remyelination by inhibiting WNT, BMP, and senescence pathways. Sci Adv. 2020;6(33):eaaz6477.
39. Guo Z, Zhang P, Chetwynd AJ, Xie HQ, Valsami-Jones E, Zhao B, et al. Elucidating the mechanism of the surface functionalization dependent neurotoxicity of graphene family nanomaterials. Nanoscale. 2020;12(36):18600-5.
40. Tu Q, Pang L, Chen Y, Zhang Y, Zhang R, Lu B, et al. Effects of surface charges of graphene oxide on neuronal outgrowth and branching. Analyst. 2014;139(1):105-15.
41. Sahiner N, Suner SS, Sahiner M, Silan C. Nitrogen and sulfur doped carbon dots from amino acids for potential biomedical applications. J Fluoresc. 2019;29(5):1191-200.
42. Sasidharan A, Panchakarla LS, Chandran P, Menon D, Nair S, Rao CN, et al. Differential nano-bio interactions and toxicity effects of pristine versus functionalized graphene. Nanoscale. 2011;3(6):2461-4.
43. Hao F, Ku T, Yang X, Liu QS, Zhao X, Faiola F, et al. Gold nanoparticles change small extracellular vesicle attributes of mouse embryonic stem cells. Nanoscale. 2020;12(29):15631-7.
44. Liang S, Zhou H, Yin N, Lu Y, Faiola F. Embryoid body-based RNA-seq analyses reveal a potential TBBPA multifaceted developmental toxicity. J Hazard Mater. 2019;376:223-32.

Figures

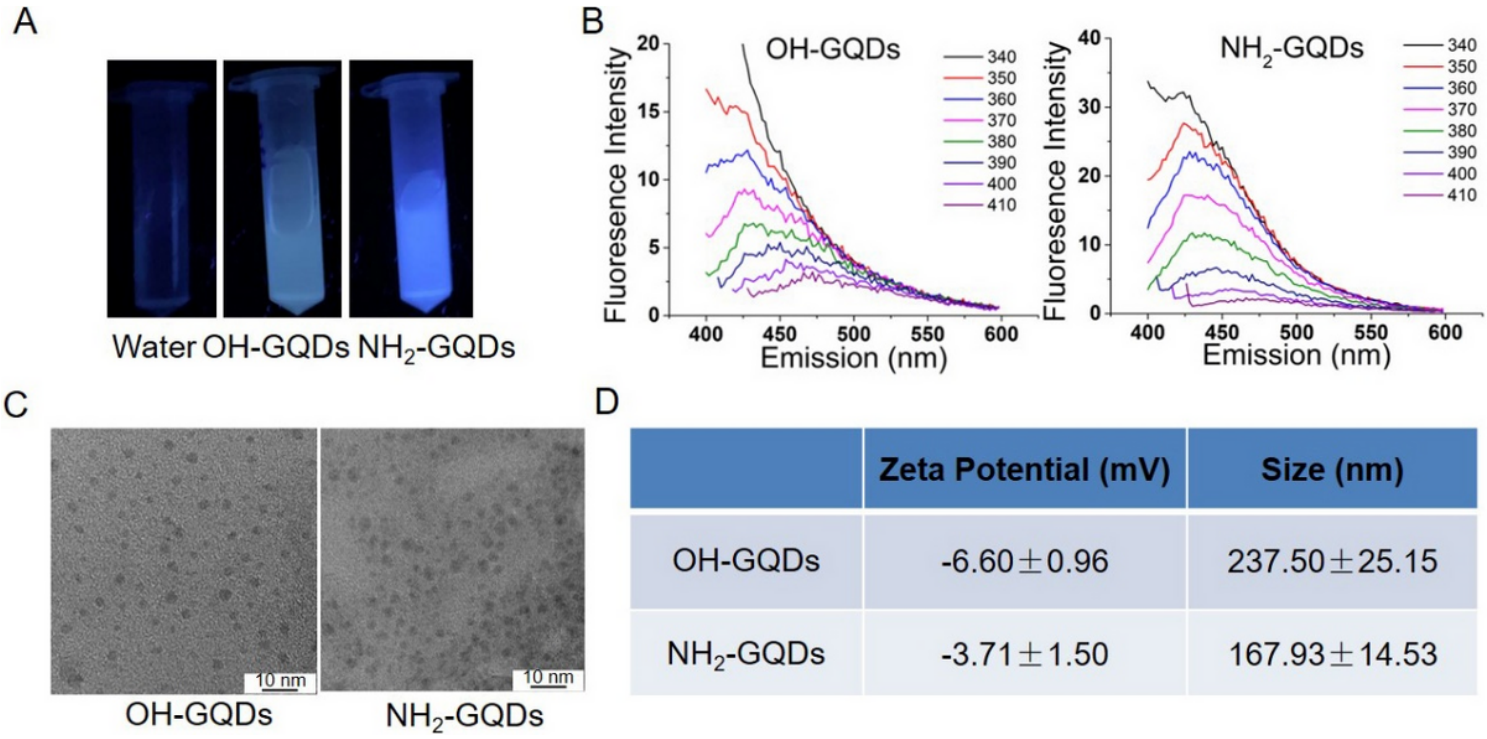

	Zeta Potential (mV)	Size (nm)
OH-GQDs	-6.60±0.96	237.50±25.15
NH_2-GQDs	-3.71±1.50	167.93±14.53

Figure 1

Characterization of OH-GQDs and NH_2-GQDs. (A) The images for the GQDs under UV illumination. (B) The fluorescence spectrum of GQDs under different excitation wavelengths. (C) The representative TEM images of OH-GQDs and NH_2-GQDs. (D) The zeta potentials and hydrodynamic diameters of OH-GQDs and NH_2-GQDs in cell culture medium.

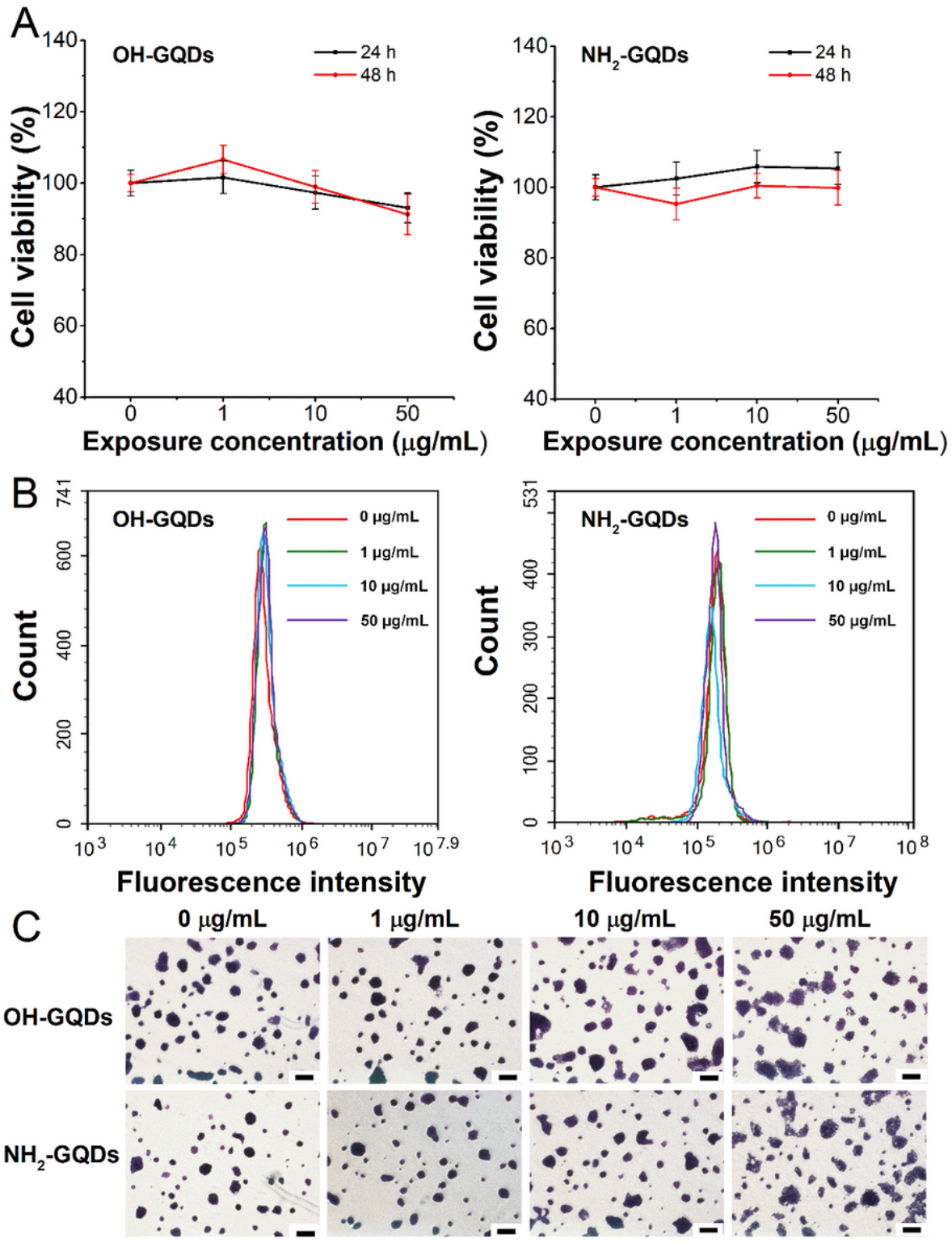

Figure 2

The cellular responses of the mESCs to GQD exposure (n = 3). (A) The cell viability by alamarBlue assay. (B) The cell proliferation by EdU incorporation assay. (C) The AP activity. Scale bar = 200 μm. *p < 0.05, **p < 0.01, or ***p < 0.001 versus the control.

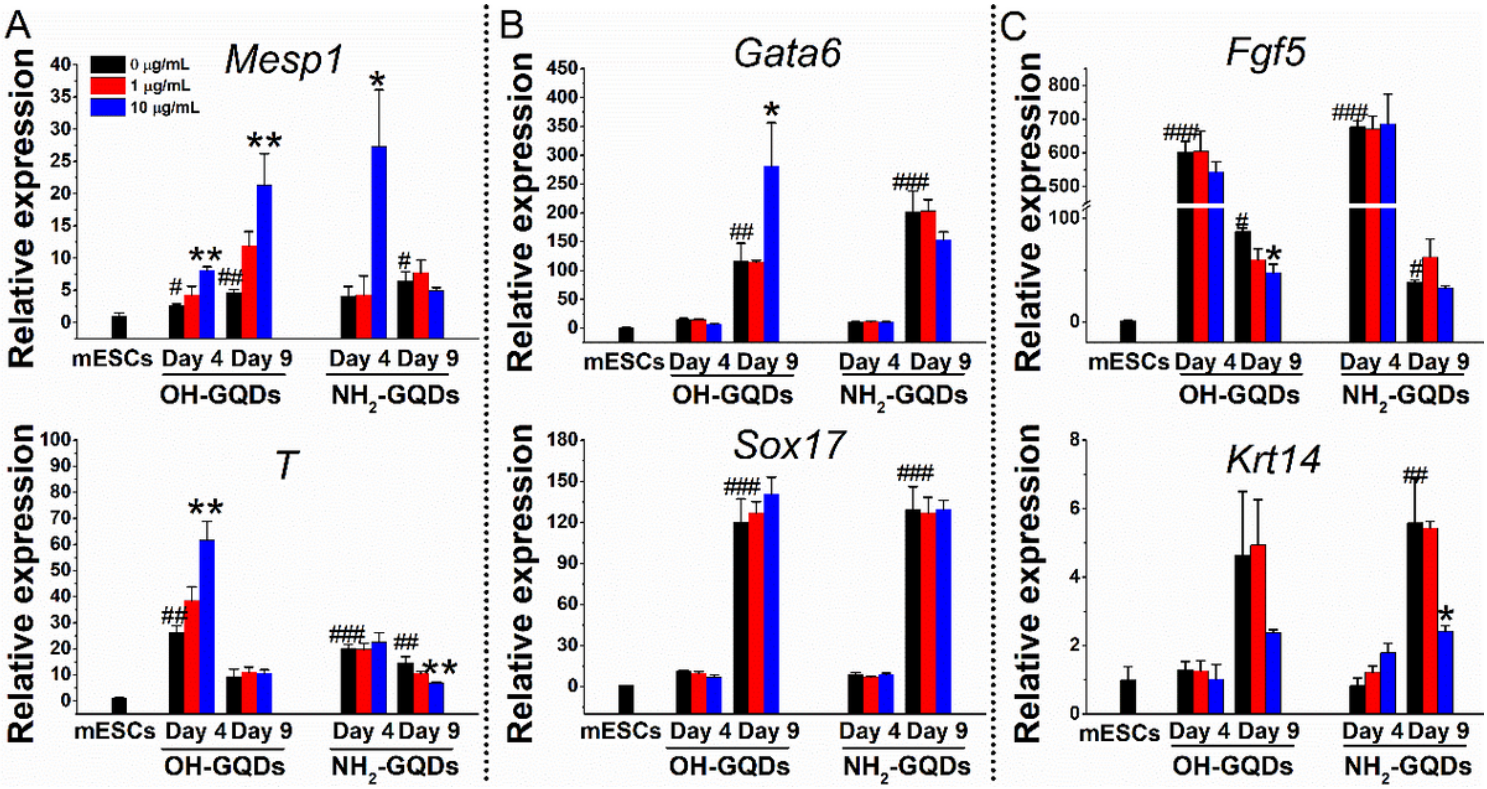

Figure 3

GQDs influenced the heterogeneous development of the mESCs (n = 3). The relative transcriptional expressions of the gene biomarkers for three germ layers of endoderm (A), mesoderm (B), and ectoderm (C). *p < 0.05, **p < 0.01, or ***p < 0.001 versus the controls at the corresponding time points. $^{\#}p$ < 0.05, $^{\#\#}p$ < 0.01, or $^{\#\#\#}p$ < 0.001 versus the mESCs.

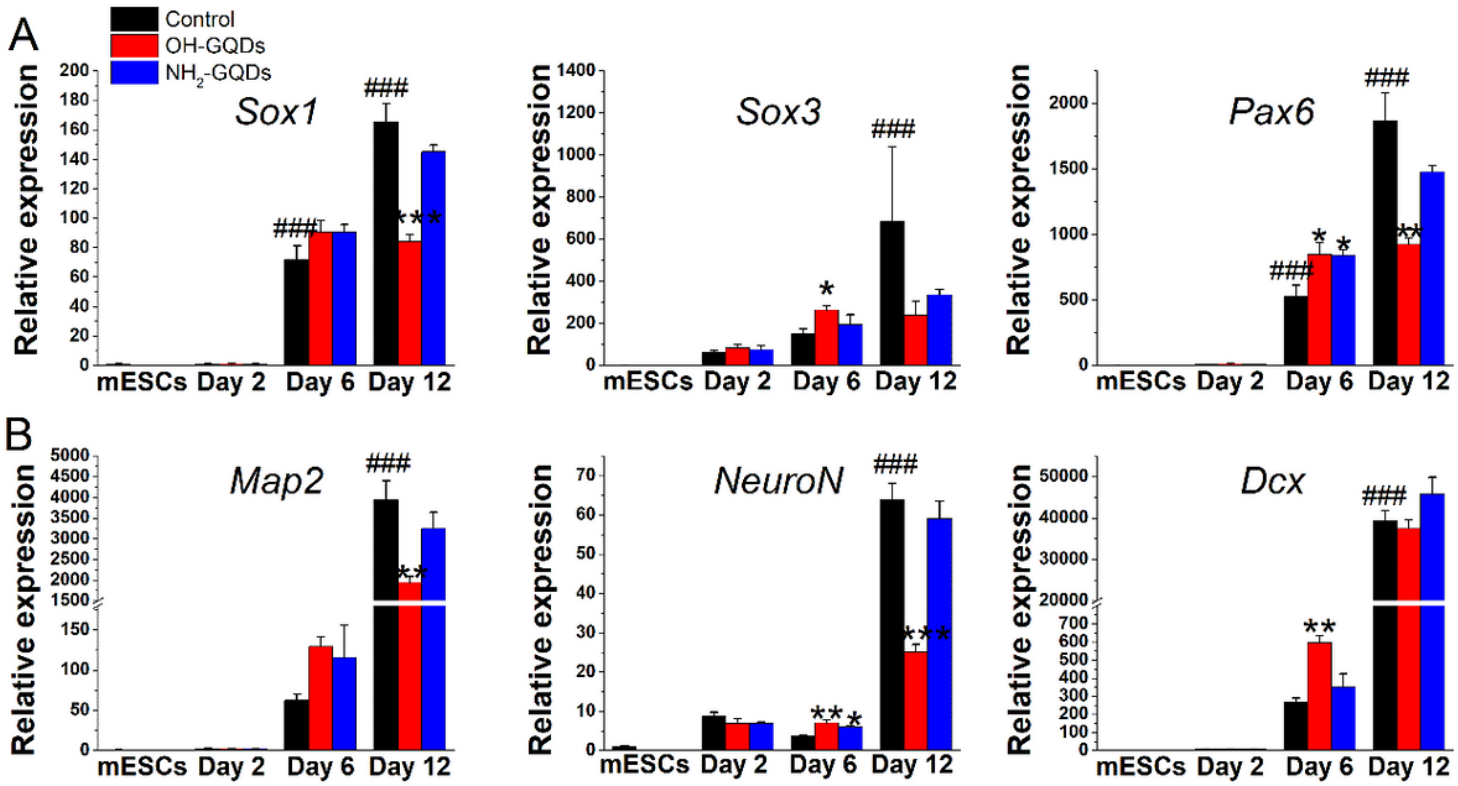

Figure 4

OH-GQDs compromised the neural differentiation of the mESCs (n = 3). The relative transcriptional expressions of the gene biomarkers for neural precursors formation (A) and neurogenesis(B). The exposure concentrations of the test GQDs were 10 mg/mL. *p < 0.05, **p < 0.01, or ***p < 0.001 versus the controls at the corresponding time points. $^{\#}p$ < 0.05, $^{\#\#}p$ < 0.01, or $^{\#\#\#}p$ < 0.001 versus the mESCs.

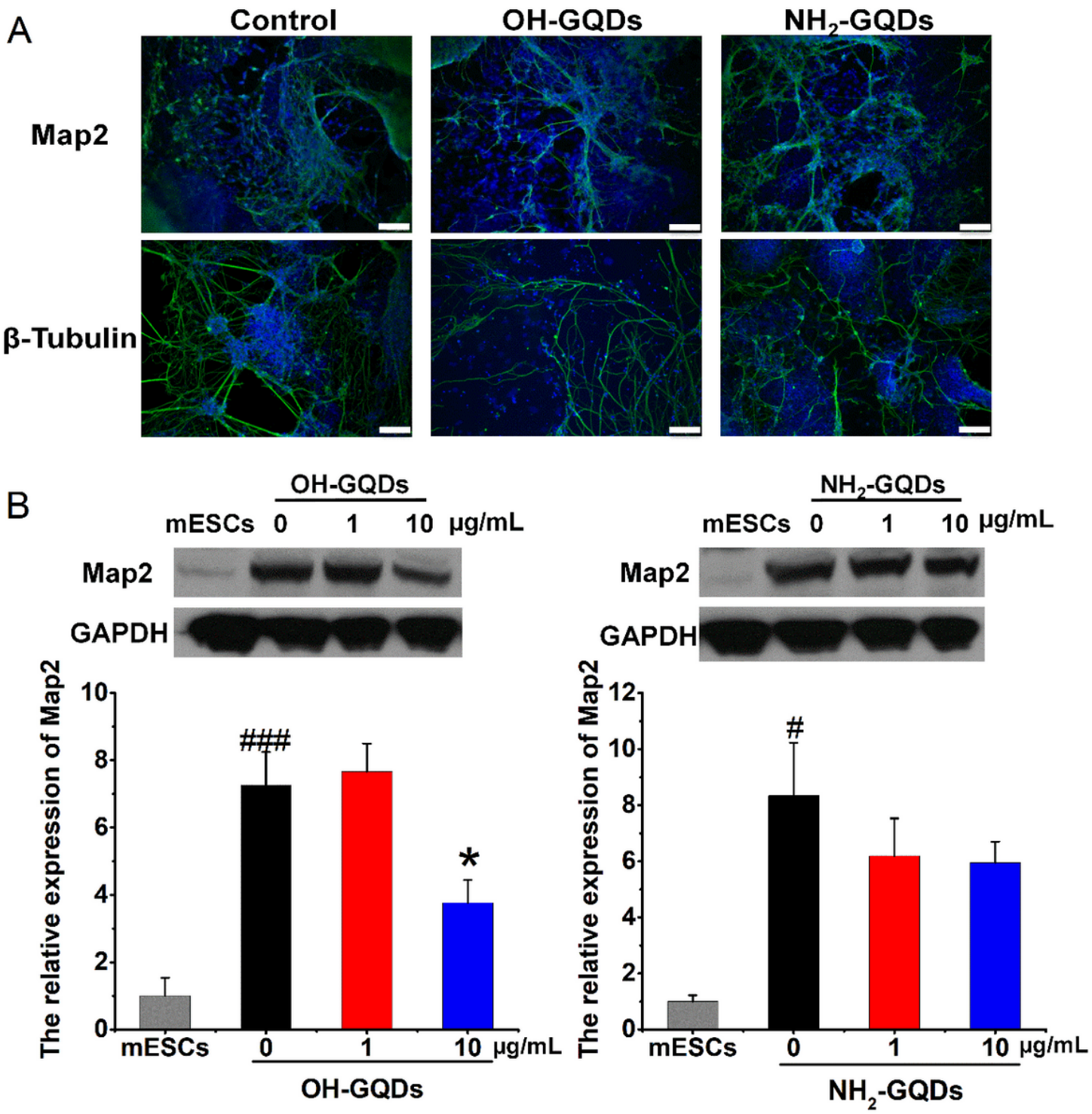

Figure 5

OH-GQDs influenced the microtubule assembly during neural differentiation. (A) Immunostaining analysis of Map2 and β-Tubulin expressions. Scale bar = 100 μm. The exposure concentrations of GQDs were 10 mg/mL. The nuclei were stained by DAPI, and the target proteins were probed by FITC. (B) Western blotting analysis of Map2 expression. The cells were harvested on differentiation day 12. *p < 0.05 versus the control group at on neural differentiation day 12. $^{\#}p$ < 0.05, $^{\#\#}p$ < 0.01, or $^{\#\#\#}p$ < 0.001 versus the mESCs.

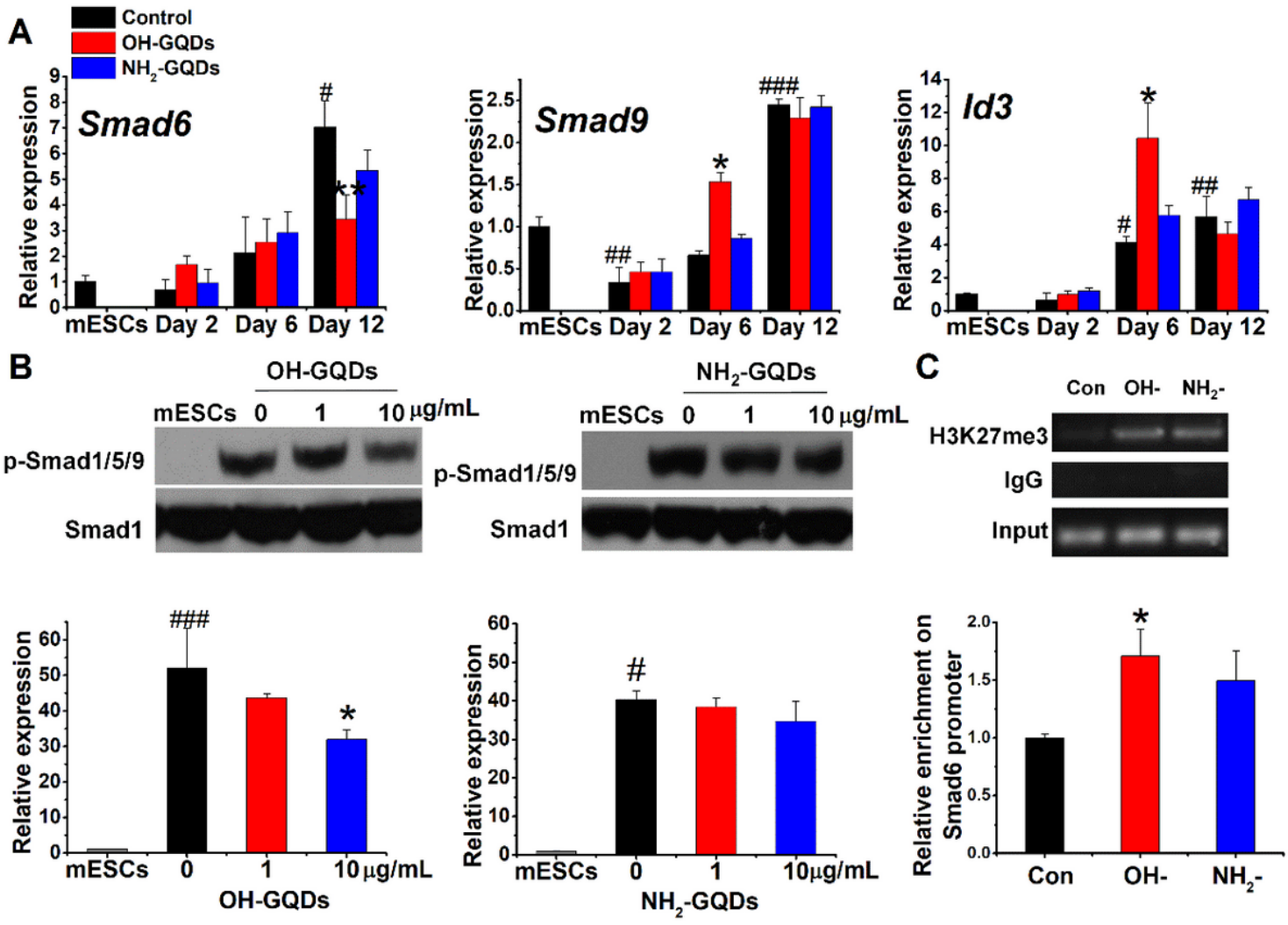

Figure 6

OH-GQDs affected BMP signaling pathway by disturbing histone modification (n = 3). (A) The relative transcriptional levels of *Smad6*, *Smad9* and *Id3*. (B) The phosphorylation of Samd1/5/9. (C) Enrichment of the H3K27me3 subunit to the promoter of *Smad6* gene. IgG was used as a negative control in the ChIP assay. The exposure concentrations of GQDs were 10 mg/mL for panel A and C, and the cells were harvested on differentiation day 12 for Panel B and C. *$p < 0.05$, **$p < 0.01$, or ***$p < 0.001$ versus the control group at on neural differentiation day 12. $^{\#}p < 0.05$, $^{\#\#}p < 0.01$, or $^{\#\#\#}p < 0.001$ versus the mESCs.

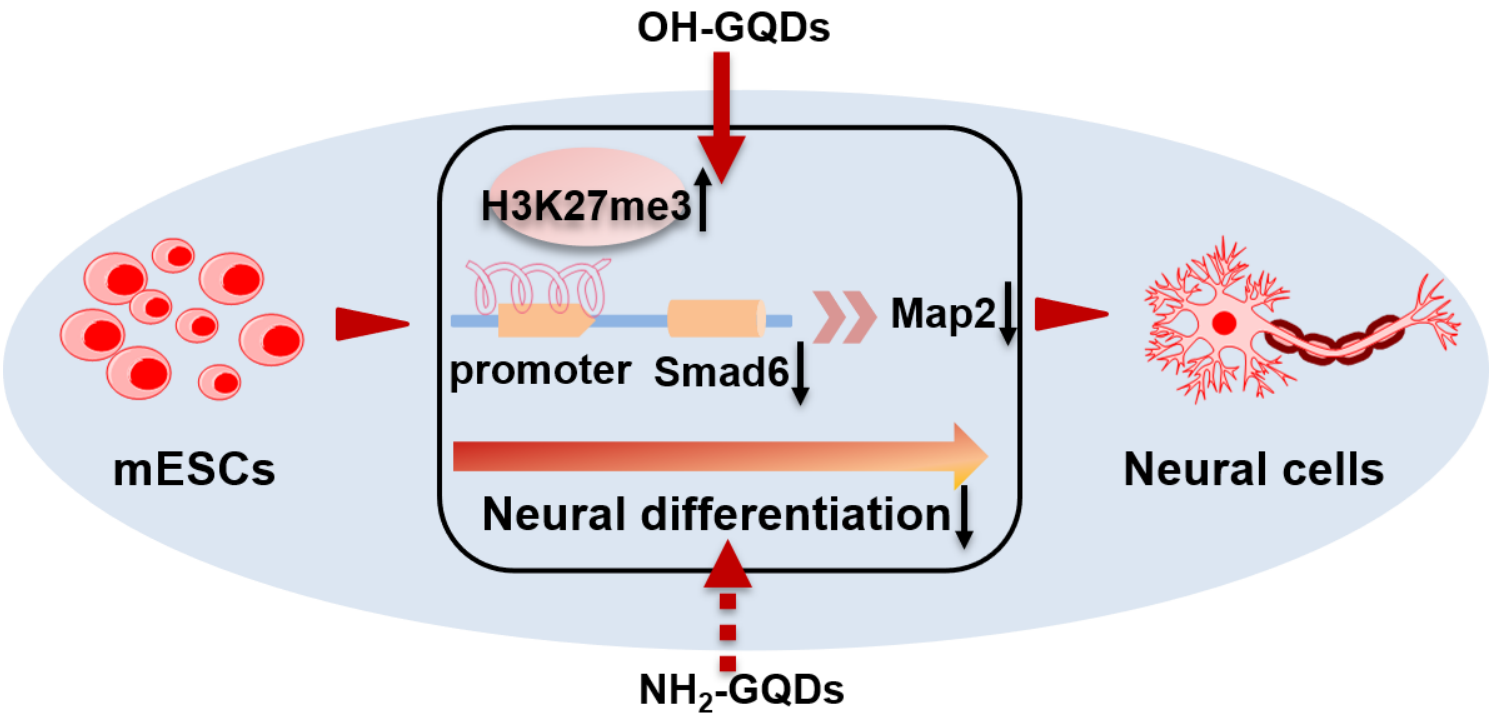

Figure 7

Schematic diagram for surface modification-specific neurodevelopment hazards of GQDs exposure.

Supplementary Files

This is a list of supplementary files associated with this preprint. Click to download.

- Supplementarymaterial1.doc
- Supplementarymaterial2.doc